strain. In consideration of the marked elastic anisotropy of α-cristobalite, it seemed essential to evaluate the directional dependence of the Poisson's ratio.

In a Cartesian coordinate system the elastic strain (e_{ij}) and the stress ($\sigma_{k\ell}$) tensors are related by

$$e_{ij} = S_{ijk\ell}\sigma_{k\ell} \quad (3)$$

The coordinate system is usually chosen to coincide with the material's principal crystallographic axes. In terms of the single-crystal elastic compliance coefficients, the quotient of lateral to longitudinal strain, $-S_{iijj}/S_{iiii}$, is the exact definition of Poisson's ratio under all possible orientations of the coordinate system relative to the crystal's axes. To calculate Poisson's ratio for an arbitrarily chosen set of axes, we transformed the elements of the compliance tensor according to standard tensor transformation rules (*5*, *15*).

In α-cristobalite the directional dependence of Poisson's ratio exhibits marked anisotropy. Over all crystallographic directions its magnitude ranges from +0.08 to −0.5, although it remains predominantly negative. Comparatively, the Reuss and Voigt bounds of the single-phased aggregate yield Poisson's ratios of −0.13 and −0.19, respectively (Table 1). Rotation of the elastic compliance tensor about the *a* axis produces a maximum $\nu_{23} = -0.5$ at approximately 42° from the *b* axis (Fig. 2B). The occurrence of this maximum can be appreciated in light of the topology of the α-cristobalite structure. As the unit cell is rotated around the *a* axis, the compressive axes become aligned with the O pair displaying the largest contractions (Fig. 2A). Compression of these O...O separations along with concomitant bending of the Si–O–Si angle result in an inward rotation of the SiO_4 tetrahedra. Consequently, the structure contracts laterally.

It is suggested that for materials having a large degree of elastic anisotropy, such as α-cristobalite, α-quartz, stishovite (the high-pressure modification of SiO_2), and $MgSiO_3$ in the ilmenite structure, whenever single-crystal elastic coefficients are available, it is valuable to carry out a tensorial analysis of the elastic coefficients and examine the entire range of behavior of Poisson's ratio.

REFERENCES AND NOTES

1. L. G. Liu and W. Bassett, *Elements, Oxides, Silicates: High-Pressure Phases with Implications for the Earth's Interior* (Oxford Univ. Press, New York, 1986).
2. H. D. Megaw, *Crystal Structures. A Working Approach* (Saunders, Philadelphia, 1973).
3. β-Cristobalite is the high-temperature polymorph of SiO_2 above 1743 K. However, β-cristobalite exists metastably to about 540 K, where it undergoes a rapid and reversible inversion to low or α-cristobalite.
4. R. Lakes, *Science* **235**, 1038 (1987).
5. D. Gunton and G. Saunders, *J. Mater. Sci.* **7**, 1061 (1972).
6. A. H. Love, *A Treatise on the Mathematical Theory of Elasticity* (Dover, New York, 1944).
7. From a thermodynamic point of view, conservation of volume is not required.
8. For details on Brillouin spectroscopy see, for example, D. Weidner and H. Carleton, *J. Geophys. Res.* **82**, 1334 (1977); M. Vaughan and J. Bass, *Phys. Chem. Miner.* **10**, 62 (1982).
9. To confirm that one of the shear waves travels with a faster velocity than the corresponding compressional wave, the polarizations of the acoustic modes were independently verified by the polarization of the scattered light according to Brillouin scattering selection rules, and by the tetragonal symmetry of the material, which requires that two modes converge to a degenerate shear mode along the *c* axis. The velocity of this shear mode is the same as the shear mode in the *a*–*b* plane, which is polarized in the *c* direction (see Fig. 1).
10. J. Nye, *Physical Properties of Single Crystals* (Oxford Univ. Press, Oxford, 1977).
11. The elasticity of a single crystal is usually described in terms of the stiffness (C_{ij}) or the compliance (S_{ij}) coefficients (the inverse of C_{ij}). The elastic compliance coefficients portray the change in the crystal's shape as it is stressed. In a crystal with tetragonal symmetry, the coefficients S_{11} and S_{33} represent the response to uniaxial compression; their magnitudes are indicative of the compressibility of the crystal along the *a* and *c* axes, respectively. The shear compliance in the *a*–*c* and *a*–*b* crystallographic planes is governed by coefficients S_{44} and S_{66}. The off-diagonal coefficients S_{12} and S_{13}, on the other hand, describe the strain induced along the *b* and *c* axes, respectively, due to a stress parallel to the *a* axis; they monitor how much a material can contract or expand laterally when compressed. A positive sign associated with these coefficients would be indicative of lateral contraction, whereas a negative sign indicates lateral expansion.
12. A. Yeganeh-Haeri *et al.*, *Eos* **71** (no. 43) (Fall Meeting Suppl.), 1671 (1991); The high-pressure crystal chemistry of SiO_2 in the α-cristobalite structure was investigated through in situ x-ray diffraction using a DIA type apparatus. Unit cell parameters were determined at ambient and elevated pressures and were then used in the distance least squares procedure to model atomic coordinates (A. Yeganeh-Haeri *et al.*, in preparation).
13. A similar expression using S_{ij} values can be written for the Reuss bounds of the aggregate.
14. In a crystal with tetragonal symmetry, $C^*_{11} = (2C_{11} + C_{33})/3$; $C^*_{44} = (2C_{44} + C_{66})/3$; $C^*_{12} = (2C_{13} + C_{12})/3$.
15. P. J. Musgrave, *Crystal Acoustics* (Holden-Day, San Francisco, 1970).

16. We thank C. Francis for providing the single crystals of α-cristobalite (Harvard Mineralogical Museum sample 97849). Financial support for this research was provided by National Science Foundation grants EAR-8804087 (D.J.W.) and DMR-9024249 (J.B.P.). Mineral Physics Institute contribution 67.

2 April 1992; accepted 22 June 1992

The Location of Bound Lipid in the Lipovitellin Complex

P. A. Timmins,* B. Poliks, L. Banaszak

The location of the bound lipid in the soluble lipoprotein lipovitellin has been determined by neutron crystallographic techniques. With the use of the contrast variation method, whereby the crystals are soaked in different H_2O-D_2O mixtures, the lipid has been found to occupy a large cavity in the protein whose structure had previously been determined by x-ray crystallography. The lipid appears to be bound in the form of a bilayer with the major protein-lipid interactions being hydrophobic and with the lipid headgroups projecting into the bulk solvent and into a solvent-filled space in the cavity.

Existing molecular models of soluble lipoproteins are based mainly on physical methods that do not permit direct visualization of molecular structure. We describe neutron diffraction results which, when combined with an earlier x-ray crystallographic study, lead to a relatively complete three-dimensional model of a soluble lipoprotein called lipovitellin. The crystalline lipovitellin complex was derived from lamprey oocytes. It is comprised of three polypeptide chains, LV1, LV2, and PV, of molecular weight (M_r) 66,800, 40,750, and 35,200, respectively. PV, sometimes also called phosvitin, contains a significant number of phosphorylated Ser residues [for a relatively recent review, see (*1*)]. In addition to the protein components, the complex contains about 15% lipid, mainly in the form of phospholipids. The lipovitellin complex has been crystallized (*2*) and its structure solved to 2.8 Å resolution by x-ray crystallography (*3*) by using classical multiple isomorphous replacement (MIR) techniques. The resulting model, however, has some important limitations that may be summarized as follows. At the time when the model was constructed, the amino acid sequence was not known and the model was therefore described as a polyalanine chain. Although the complex is known to comprise ~1300 amino acids, the initial interpretation of the electron density based on multiple isomorphous replacement (MIR)

P. A. Timmins, Institut Laue-Langevin, 156X, 38042 Grenoble, Cedex 9, France.
B. Poliks, Department of Biological Chemistry, Washington University Medical School, St. Louis, MO 63110.
L. Banaszak, Department of Biochemistry, University of Minnesota Medical School, Minneapolis, MN 55455.
*To whom correspondence should be addressed.

phases accounted for 984 residues, indicating that part of the protein was probably disordered in the crystal lattice. In particular, no elevated density corresponding to phosphoprotein was observed. In the study reported here, we used a model containing a further 26 residues located in the density after the application of solvent leveling procedures (*4*). Most important, no electron density assignable to phospholipid was visible in the x-ray study. In order to locate the phospholipid in the crystallographic model and search for the missing segment of phosphoprotein, neutron diffraction experiments were carried out with lipovitellin single crystals along with the H_2O-D_2O contrast variation method [reviewed in (*5*)]. The results show that the lipid moiety is bound within a large cavity in the structure bounded by presumably hydrophobic side chains located on the nearby β structure. Furthermore, the protein not accounted for in the x-ray maps, which was believed to be part of the PV chain, is extremely disordered. The contrast variation study suggests that the missing segment of phosphoprotein occupies a part of the solvent volume of the crystal as discerned in the electron density map.

The lack of lipid density in the x-ray maps must be due to disorder in the phospholipid. In this case, the contrast that would produce scattering at low resolution (> ~10 Å) would be due to the difference in average electron density between lipid and water. As the mean electron density of both these moieties is ~0.334 e $Å^{-3}$, the contrast is zero or very small and lipid is therefore indistinguishable from the solvent water in the crystal. In the case of neutron scattering, the contrast depends very strongly on the H_2O-D_2O content of the solvent and for the various components of lipovitellin is illustrated in Fig. 1. These variations are due to the difference in scattering length between H (-0.374×10^{-12} cm) and D (0.667×10^{-12} cm).

The contrast variation method can be used to identify lipid, protein, and phosphoprotein in any crystalline system containing these components. If a partial structure is known from x-ray studies, the determination of a low-resolution structure based on neutron diffraction data should be feasible. The case of lipovitellin is rather unfavorable as only some 78% of the protein structure is known, and in the absence of a fitted amino acid sequence this can only be modeled as a homogeneous scattering density. The neutron scattering ability of each amino acid type varies differently with D_2O concentration and is particularly sensitive to the ratio of exchangeable hydrogens to nonexchangeable hydrogens.

For lipovitellin, crystals similar to those used for x-ray studies were used to obtain neutron diffraction data. The details of data collection, processing, scaling, and phasing are given in Tables 1 and 2. For neutron scattering, calculations based on chemical composition show that protein and phospholipid are matched by solvent in the crystal interstices at solvent compositions of ~40 and 10% by mole D_2O, respectively. Hence in a scattering density map with 40% D_2O one would expect to see mainly

Table 1. Lipovitellin data collection statistics. Crystals for neutron diffraction (maximum dimensions 1.0 mm by 0.5 mm by 0.5 mm) were soaked for ~3 weeks in 0.6 M sodium citrate, pH, 6.4, made up in D_2O-H_2O mixtures as indicated in the upper part of the table. Exact D_2O contents were obtained from neutron transmission measurements. The crystals used are very small compared with those necessary for high-resolution neutron crystallography and are sufficient for two prime reasons: (i) the low-resolution diffraction is inherently strong; and (ii) the use of long-wavelength neutron radiation (7.56 Å) leads to a high crystal reflectivity and hence large measured intensities. The neutron diffraction data were collected to 12 Å resolution on the diffractometer DB21 at the high-flux reactor of the Institut Laue-Langevin, Grenoble, France. The incident beam consisted of a monochromatic beam of neutrons of wavelength 7.56 Å, which are detected on a two-dimensional Li/Ce scintillator detector (*7*). Data collection times varied between 5 and 14 days depending on the D_2O-H_2O contrast. Crystals undergo no radiation damage from neutron irradiation.

D_2O content (% by mole)	Total reflections (no.)	Unique reflections (no.; % possible)	R_{merge}*
0	970	424 (88)	0.054
20	858	457 (96)	0.044
59	1086	431 (92)	0.038
85	690	386 (82)	0.018
93	1031	484 (100)	0.014

*$R_{merge} = \Sigma|I - \langle I \rangle|/\Sigma I$, where I is the intensity of a reflection and the sum is over all observed reflections.

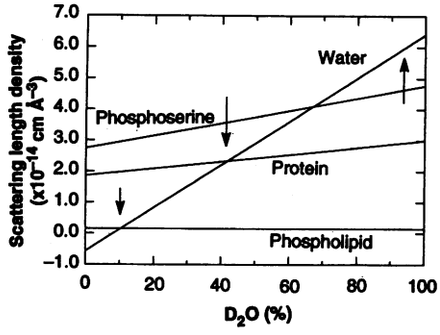

Fig. 1. Contrast variation for neutron diffraction studies of lipovitellin. Variation of scattering length density of various components of lipovitellin are shown as a function of D_2O content of the surrounding solvent. The point at which the scattering length density of a component equals that of the solvent is the contrast match point. Note that the scattering length densities are calculated for "dry" molecules. If the molecule is disordered such that the volume that it occupies is also partially occupied with water, then the corresponding scattering length density is reduced so that in the high-dilution limit it is equal to that of the mother liquor. This reduction in absolute scattering density, however, does not change the contrast match point, which is only a function of the chemical composition. The optimum contrast at which to view, for example, phosphoprotein remains that at which normal protein is matched by the solvent. Note especially that at 40% D_2O, the most negative density is attributable to lipid. The arrows indicate the contrasts at which final maps were calculated.

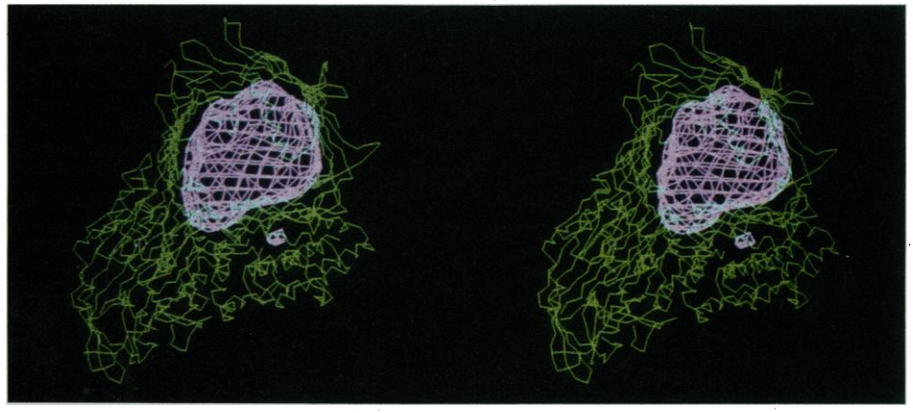

Fig. 2. Crystalline lipovitellin at 40% D_2O. The stereodrawing shows the neutron scattering length density map in 40% D_2O contoured at 1.5σ (where σ is the root-mean-square neutron scattering length density) and superimposed upon an α-carbon trace representing the protein model in green. The model is that determined by x-ray crystallography (*3*). The negative density shown in violet at this contrast indicates the presence of phospholipid. Small areas of density within the protein are probably due to clumps of hydrophobic amino acids, which also have negative contrast in 40% D_2O.

phospholipid at high negative contrast and in 10% D_2O to see predominantly protein at high positive contrast. Because of the presence of phosphoserines in the phosvitin chain, one would expect to see portions of this polypeptide component at positive contrast in the 40% D_2O map. In 93% D_2O, all of the lipovitellin components would be at negative contrast, with lipid having ~1.8 times the contrast of protein.

The map at 40% D_2O, along with the polypeptide chain trace of lipovitellin from the x-ray studies, is shown in Fig. 2. The most striking feature is the presence of continuous high negative density in the central cavity formed by the β-sheet domains. The volume of this negative region is of course dependent on the contouring threshold, but if we use levels as shown in Fig. 2, the cavity density is equivalent to ~28,000 Å^3. If we assume that at this contrast we are seeing primarily the acyl chains of the phospholipid, the neutron scattering cavity is large enough to accommodate ~32 molecules of phospholipid. Therefore the neutron diffraction results are in general agreement with the amount of lipid known to be present based on chemical analyses (*2*). A few regions of small volume containing negative density not visible in Fig. 2 are probably due to scattering length density fluctuations within the protein. The starting model, which consisted only of homogeneous polyalanine, was modulated by the density modification scheme.

Another nearly orthogonal view of the

Table 2. Lipovitellin phase estimation. The data were scaled together using a procedure (*8*) that also enables the D_2O contents to be refined. Once the data are scaled together, structure factor (*F*) amplitudes for any contrast can then be interpolated from the general relation that relates structure factor to contrast (*9*). We chose to work with data from contrasts corresponding to 10% D_2O, where lipid is on average matched out, 40% D_2O, where protein is on average matched with the solvent, and 93% D_2O, which was the highest measured contrast. Starting phases for the neutron data in 10% D_2O were obtained by calculation from the x-ray coordinates. We assumed that each amino acid has the volume and scattering power of an average amino acid, that is, a volume of 133 Å^3 and a scattering power in H_2O of 2.4 × 10^{12} cm, which varied with D_2O because of the presence of 1.8 exchangeable hydrogen atoms. The *R* values for the starting model are shown. That for 40% D_2O is indeterminate as the structure factors are zero because the model protein has no contrast at this point. The starting model was combined with the contrast variation to produce a "best" map at the three chosen contrasts in a fashion analogous to that of single isomorphous replacement (*10*). The 40% D_2O best map already showed significant density in the cavity. The best maps were then improved by density modification using a suite of programs written by Roth (*11*). The envelope used for density modification was an F_{calc} α_{calc} map calculated from the x-ray coordinates. For example, a fraction of 15% of the most negative density in the 40% D_2O map was extracted and used as a model for the lipid. A similar procedure was applied to the 93% D_2O map where the lipid model was recombined through the structure factors with the structure factors calculated from the x-ray model at that contrast. After solvent leveling, these models were then reused for calculating "best" maps and the process cycled until no significant improvement of *R* factor was obtained.

D_2O content (% by mole)	*R* value*		Figure of merit‡	
	Initial†	Final	Initial§	Final
10	0.43	0.29	0.747	0.835
40		0.34	0.542	0.828
93	0.71	0.36	0.638	0.861

*$R = \Sigma|F - F_{obs}|/\Sigma F_{obs}$, where $F = F_{calc}$ for initial and $= F_{best}$ for final. †From x-ray crystallographic coordinates. ‡Figure of merit is the average of the cosine of the difference in phase difference between the value calculated from the model and that determined from the contrast variation experiment for the contrast under consideration with respect to a reference contrast. §After first F_{best} calculation.

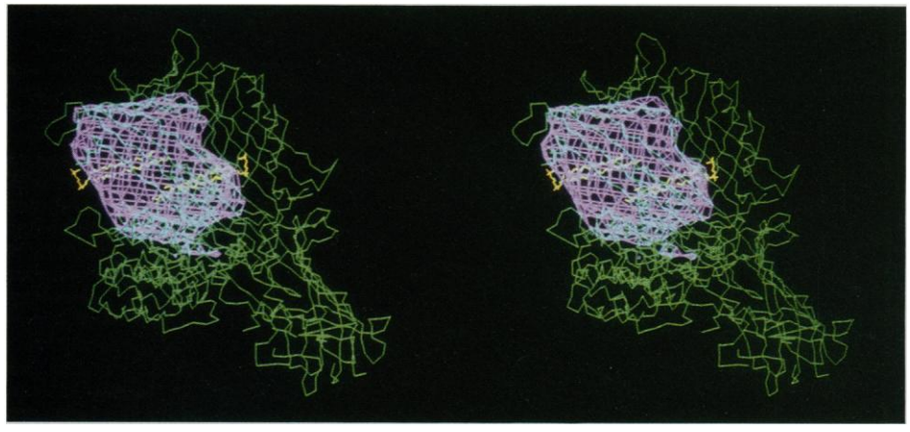

Fig. 3. The lipid cavity in lipovitellin. The stereodrawing contains the same map as is shown in Fig. 2 viewed from a direction perpendicular to the dimer interface. The negative neutron scattering as seen by the violet contours can be compared with the crystallographic model in green. It is apparent in this view that the lipid density is located mostly toward the open end of the cavity while there is very little negative density in the region adjacent to the dimer interface. The lipovitellin dimer interface is formed by the single α helix and its symmetry-related mate, which is not shown. Two phospholipid molecules have been inserted into the density to show how such molecules might pack into the cavity. The two phospholipid molecules illustrated here represent C_{16}-C_{18} phosphatidylcholine. In the lipovitellin complex, a mixture of different phospholipids, along with a small amount of neutral lipids, is present. The molecules have been placed such that their acyl chains are in the negative density defined by the neutron diffraction studies and their polar headgroups protrude into the aqueous regions on either side.

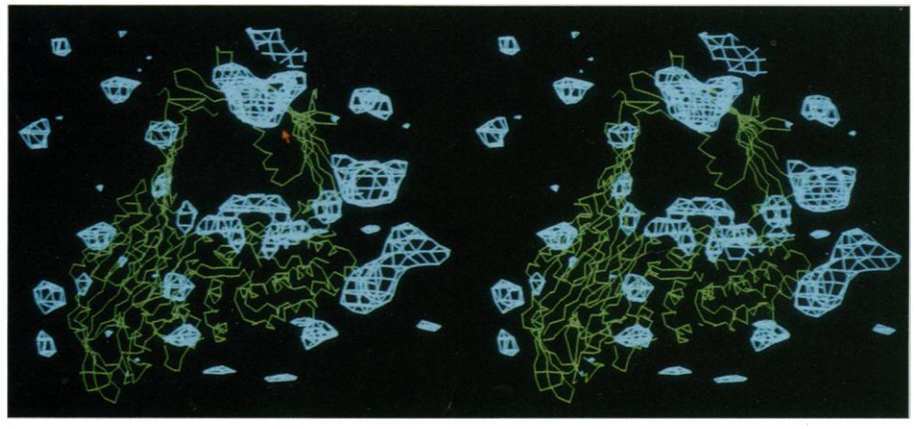

Fig. 4. Positive neutron scattering density at 40% D_2O. The stereodrawing contains the positive neutron scattering density of lipovitellin shown in light blue contoured at 1.3σ. The positive density at this contrast indicates either hydrophilic amino acids or segments of the phosphoprotein. The contoured region indicated by a red arrow is at the interface between the two constituent monomers of the dimer and may be an extension of the α helices that in the x-ray model are the main elements of this interface (see text).

cavity (Fig. 3) shows that the density does not entirely fill the cavity as defined by the x-ray model. Although only a monomer is shown in Fig. 3, the area of the cavity region close to the dimer interface has very little density associated with it. This is the part of the cavity that is formed mainly by two opposing α helices from different subunits. It is marked in the x-ray model of Fig. 3 by the single α helix forming a backdrop to the cavity region. The neutron maps at 10% D_2O and 93% D_2O (not shown) also indicate a similar lack of density, which suggests that this region is either full of solvent or more probably that it is the location of highly hydrated lipid headgroups, which have very little contrast.

The two phospholipid molecules placed in the negative density in Fig. 3 show a hypothetical packing arrangement within the lipoprotein complex. In the scattering length density of the 93% D_2O map, where the highest contrast arises from close-packed acyl chains, the density in the cavity merges smoothly into the β sheet of the surrounding protein. This is strong evidence for the major interaction between lipid and protein to be through hydrophobic contacts. If the interaction were through hydrated phospholipid headgroups, one would expect to see a very low density region in contact with the protein. Two molecules of phospholipid are shown to indicate that the size of the neutron cavity is sufficient to accommodate a microdomain of phospholipid bilayer. Based on ^{31}P nuclear magnetic resonance studies, the possibility that the phospholipid in lipovitellin is in such an anisotropic environment has been suggested (6).

It was hoped that the neutron diffraction studies would also indicate the location of the phosphorylated segment of phosvitin. As noted above, the x-ray model is not complete because no electron density was found to suggest the position of phosphorylated side chains. The prediction is that a component containing mainly phosphoserine would appear as positive contrast in a 40% D_2O map as can be seen in Fig. 1.

The regions of positive contrast in the 40% D_2O map are shown in Fig. 4, again along with the x-ray model. There are only three larger regions of density that have a higher contrast than normal protein. One of these regions appears to be an extension of the α helix that forms the dimer interface and may therefore mediate closer contacts between the lipovitellin monomers. There is little to be said about the other two positive regions except that they are located in solvent channels within the crystal lattice. They occupy volumes outside of the existing x-ray model. In addition to these three larger positive peaks, numerous small positive peaks, again all outside of the x-ray model, are also visible in Fig. 4. Without the indication of a single aggregate site in this positive density, speculation about the location of the missing phosphoprotein is difficult. The simplest explanation in agreement with the appearance of the positive neutron scattering peaks at 40% D_2O suggests either that it is located in one of the three larger positive peaks or that the missing phosphoprotein is probably highly disordered and hydrated.

The contrast variation technique, when used in conjunction with single-crystal diffraction, predicts the location of the phospholipid within the molecular model of lipovitellin derived from x-ray studies. Although the resolution is only at 12 Å, the neutron-defined lipid cavity is located in a region that was unoccupied in the x-ray model. We have therefore demonstrated that in lipovitellin the stored phospholipid is located in a cavity in the protein formed primarily by β-sheet structure. We suggest that the lipid is stabilized through hydrophobic interaction with the presumed apolar face of the juxtaposed β sheets.

REFERENCES AND NOTES

1. L. Banaszak, W. Sharrock, P. A. Timmins, *Annu. Rev. Biophys. Biophys. Chem.* **20**, 221 (1991).
2. T. Meininger, R. Raag, S. Roderick, L. J. Banaszak, *J. Mol. Biol.* **179**, 759 (1984).
3. R. Raag, K. Appelt, N.-H. Xuong, L. J. Banaszak, *ibid.* **200**, 553 (1988).
4. B. Poliks and L. Banaszak, unpublished results.
5. P. A. Timmins and G. Zaccai, *Eur. Biophys. J.* **15**, 257 (1988).
6. L. J. Banaszak and J. Seelig, *Biochemistry* **21**, 2436 (1982).
7. C. T. Roche, M. G. Strauss, R. Brenner, *IEEE Trans. Nucl. Sci.* **NS-32**, 373 (1985).
8. M. Roth, A. Lewit-Bentley, G. A. Bentley, *J. Appl. Crystallogr.* **17**, 77 (1984).
9. M. Roth, *Acta. Crystallogr.* **A43**, 780 (1987).
10. D. L. Worcester and N. P. Franks, *J. Mol. Biol.* **100**, 359 (1976).
11. M. Roth, in *Crystallographic Computing 5*, D. M. Moras, A. D. Podjarny, J. C. Thierry, Eds. (Oxford Univ. Press, Oxford, in press).

12. We are extremely grateful to M. Roth (LIP, Grenoble) for making available several of the programs used in this study as well as for discussions on their applications. We also thank P. Metcalf (EMBL, Heidelberg) for his help in the early stages of this work. Supported in part by grants from NIH (to L.J.B.) and NATO (to L.J.B. and P.A.T.).

27 February 1992; accepted 29 May 1992

Vacuolar Chitinases of Tobacco: A New Class of Hydroxyproline-Containing Proteins

Liliane Sticher, Jan Hofsteenge, Alfred Milani, Jean-Marc Neuhaus, Frederick Meins, Jr.*

The fungicidal type I chitinases contribute to the defense response of plants against pathogens. Two tobacco chitinases represent a different class of hydroxyproline-containing proteins. Hydroxyproline-rich proteins are predominantly extracellular, structural glycoproteins that lack enzymatic activity and contain many hydroxyproline residues. In contrast, type I chitinases are vacuolar enzymes. They are not glycosylated and contain a small number of hydroxyproline residues restricted to a single, short peptide sequence.

Hydroxylation of prolyl residues is an important posttranslational modification of some secreted structural proteins. In animals, the major hydroxyproline-containing protein (HCP) is collagen, in which hydroxyproline residues are essential for stabilizing the triple-helix structure of the molecule (*1*). In plants, several secreted structural glycoproteins contain hydroxyproline (*2*): the hydroxyproline-rich glycoproteins (HRGPs) or extensins, which are components of cell walls with chains of one to four arabinoses O-linked to hydroxyproline; the arabinogalactan proteins (AGPs), which are soluble proteins and have polymers of galactose and arabinose O-linked to hydroxyproline; and certain lectins of solanaceous plants, with O-glycosylated hydroxyproline in domains structurally similar to HRGPs. The 4-*trans*-hydroxyproline (4Hyp) and the less common 3-*trans*-isomer found in HCPs result from the posttranslational hydroxylation of peptidyl prolines present in repeated peptide motifs such as GPPG (*3*) in collagens (*4*), SPPPP in HRGPs, and APA in AGPs (Table 1).

Here, we show that the type I tobacco chitinases CHN-A and CHN-B are HCPs. Type I chitinases are vacuolar proteins (*5*) implicated in the defense of plants against pathogens (*6*). The mature tobacco isoenzymes consist of a conserved lectin domain linked to the catalytic domain by a short spacer rich in T, P, and G residues (*7*, *8*). The primary structures of the isoforms differ by only three conservative substitutions and a deletion of five amino acids in the spacer (Fig. 1).

L. Sticher, J. Hofsteenge, A. Milani, F. Meins, Jr., Friedrich Miescher-Institut, CH-4002 Basel, Switzerland.
J.-M. Neuhaus, Botanisches Institut, Abt. Pflanzenphysiologie, CH-4056 Basel, Switzerland.

*To whom correspondence should be addressed.